Optimal thermoelectric figure of merit in Bi_{2}Te_{3}/Sb_{2}Te_{3} quantum dot nanocomposites

Jun Zhou, Yuanyuan Wang, Jeff Sharp, and Ronggui Yang

Phys. Rev. B **85**, 115320 — Published 29 March 2012

DOI: 10.1103/PhysRevB.85.115320

Optimal Thermoelectric Figure of Merit in Bi_2Te_3/Sb_2Te_3 Quantum Dot Nanocomposites

Jun Zhou,[1] Yuanyuan Wang,[1] Jeff Sharp,[2] and Ronggui Yang[1,*]

[1]Department of Mechanical Engineering, University of Colorado,

Boulder, Colorado 80309, USA

[2]Marlow Industries, Dallas, Texas 75238, USA

Following the idea that there exists an optimal bandwidth for maximizing the thermoelectric figure of merit (ZT), we conduct detailed calculations in this paper to search for the optimal ZT in Bi_2Te_3/Sb_2Te_3 quantum dot (QD) nanocomposites (NCs) with Bi_2Te_3 QDs uniformly embedded in Sb_2Te_3 matrix where electron minibands are formed. The two-channel transport model, which considers both the miniband transport by the quantum-confined carriers and the background transport by the bulk-like carriers, is used for electrical transport, while the lattice thermal conductivity is modeled using the modified effective medium approximation. Simultaneous decrease of the lattice thermal conductivity and the Lorenz number leads to an enhanced ZT in QD NCs when the Seebeck coefficient is not dramatically decreased. The optimal structural parameters that result in optimal electronic structure for maximizing ZT are found, with the consideration of realistic carrier scattering physics including phonon bottleneck effect. The optimal QD size is found to be ~ 6 nm, and the optimal inter-dot distance depends on the QD size and the doping concentration. For a

* Author to whom correspondence should be addressed: Ronggui.Yang@colorado.edu

given QD size, the maximum ZT is determined by the minimum of Lorenz number, which occurs when the quantum-confined carrier transport overwhelms the bulk-like carrier transport.

Keywords: thermoelectrics, nanocomposites, quantum dot, electronic band structure, Lorenz number

PACS numbers: 72.10.-d, 72.20.Pa, 73.63.Kv

I. INTRODUCTION

Thermoelectric (TE) refrigeration and power generation devices that directly convert between heat and electricity without a need for low-reliability moving parts or environment-damaging working fluids are of great interest for waste heat recovery, solar energy utilization, thermal management of electronics, and utility-scale refrigeration.[1,2] The energy conversion efficiency of TE devices is determined by the dimensionless figure of merit (ZT) of the material,[3]

$$\mathrm{ZT} = \frac{\sigma S^2}{\kappa_e + \kappa_p} T \,, \tag{1}$$

where σ is the electrical conductivity, S is the Seebeck coefficient, T is the absolute temperature, κ_e is the electronic thermal conductivity, and κ_p is the lattice thermal conductivity. Over the past two decades, there have been two main routes exercised to enhance ZT. One is to reduce the lattice thermal conductivity through nanostructuring by scattering of phonons using interfaces[4,5,6,7,8,9,10,11,12] or through filling cage-like atomic structures, such as those found in skutterudites and clathrates, with heavy rattling atoms,[13,14] and the other is to optimize the electronic transport properties.[15,16,17,18,19] When the optimized power factor (σS^2) of a TE material is reported, the simultaneous change of electronic thermal conductivity is often overlooked. Indeed, the optimal value of the Seebeck coefficient in good TE materials is rather limited, usually in the range of $200 - 230\ \mu\mathrm{V/K}$, because only the carriers distributed within a few $k_B T$ around the chemical potential contribute to transport.[20] A more feasible way to enhance power factor should come from the increase of the electrical conductivity. However, increasing electrical conductivity usually results in an increase of electronic thermal conductivity since these two transport properties are

proportional to each other. The power factor and thermal conductivity cannot be separately optimized because the electronic thermal conductivity and lattice thermal conductivity are usually similar in magnitude in good TE materials.[8,9]

We can rewrite the TE figure of merit ZT in Eq. (1) as:

$$\mathrm{ZT} = \frac{S^2}{L + \frac{\kappa_p}{\sigma T}}, \tag{2}$$

where L is the Lorenz number. It is obvious that both small $L + \frac{\kappa_p}{\sigma T}$ and large S are preferred to obtain large ZT. In Eq. (2), the Lorentz number can be written as:

$$L = \kappa_e / \sigma T \propto \frac{1}{\langle \Xi(E) \rangle} \left[\left\langle (E-\mu)^2 \Xi(E) \right\rangle - \frac{\left\langle (E-\mu)\Xi(E) \right\rangle^2}{\langle \Xi(E) \rangle} \right], \tag{3}$$

where E is the energy of the carriers, $\Xi(E) \sim v_x^2(E)\tau(E)N(E)$ is the transport distribution function (TDF), $v_x(E)$ is the carrier velocity along transport direction, $\tau(E)$ is the carrier relaxation time, $N(E)$ is the carrier density of states (DOS), μ is the chemical potential, and the bracket $\langle \cdots \rangle$ denotes the statistical average weighted by $[-df(E)/dE]$ over all the carriers; for example, $\langle \Xi(E) \rangle \sim \int dE[-df(E)/dE]\Xi(E)$ where $f(E)$ is the equilibrium Fermi-Dirac distribution. The Lorenz number is usually a constant of $2.45 \times 10^{-8}\,\mathrm{W\Omega/K^2}$ for degenerate carriers in bulk metals, with a similar value in highly doped semiconductors, as dictated by the Wiedemann-Franz Law.[21] On the other hand, the Lorenz number has been found to be much smaller in low-dimensional materials such as InGaAs/InGaAlAs supperlattices[22] and Pt nanowires[23] due to the change of the doping concentrations and the scattering mechanisms. From the Cauchy-Schwarz inequality [24] $\left\langle \Xi(E)\phi^2(E) \right\rangle \left\langle \Xi(E)\varphi^2(E) \right\rangle \geq \left\langle \Xi(E)\phi(E)\varphi(E) \right\rangle^2$ with $\phi(E) = E - \mu$ and $\varphi(E) = 1$, one can

easily find that $L = 0$ is possible when the equal-sign holds. It is thus attractive to find a typical functional form of $\Xi(E)$ that can lead to $L = 0$ and $\langle \Xi(E) \rangle \sim \sigma \neq 0$ to maximize ZT.

In 1996, Mahan and Sofo[15] originally pointed out that $L = 0$ and $\sigma \neq 0$ could be found in an electronic structure with a delta-shaped TDF $\Xi(E) \sim \delta(E - E_0)$. However, such an electronic structure does not exist in any realistic material systems, even though the original idea is mathematically rigorous. Recently, we revisited this problem by studying the TE transport in a narrow conduction band using the tight-binding model along with a few most-used carrier scattering models.[25] We found that the optimal ZT cannot be obtained in an extremely narrow conduction band with zero energy variation of $\Xi(E)$. However, there exists an optimal bandwidth with nonzero energy variance of $\Xi(E)$ for maximizing ZT, but such an optimal bandwidth depends strongly on the scattering mechanisms and the lattice thermal conductivity.

In this work, we use the findings of Ref. 25 to search for optimal ZT in Bi_2Te_3/Sb_2Te_3 quantum dot (QD) nanocomposites (NCs). In Bi_2Te_3/Sb_2Te_3 QD NCs, electronic minibands are formed[26,27,28,29] due to the hopping mechanism of quantum-confined carriers whose bandwidths are tunable through changing the size of QD and the inter-dot distance. However, more detailed calculations beyond Ref. 25, including the background transport besides the narrow minibands of quantum-confined carriers and the carrier relaxation time that accounts for the detailed scattering mechanisms, need to be performed for this realistic material system. Regarding to electrical transport, we have recently established a two-channel electrical transport model for QD NCs,[29] which includes both the transport of quantum-confined

carriers and the semi-classical transport of bulk-like carriers. This two-channel transport model enables us to study the dependence on the QD size and inter-dot distance (bandwidth tunability) of the TE transport properties in QD NCs. Along with the findings of Ref. 25, the objective of this work is to study the optimal ZT in Bi_2Te_3/Sb_2Te_3 QD NCs in the presence of both quantum-confined carrier miniband transport and the background transport by the bulk-like carriers.[29]

This paper is organized as follows. In Sec. II, we briefly present the two-channel electrical transport model for QD NCs, the modified effective medium model for lattice thermal conductivity, and the material input parameters for the calculations. In Sec. III, we first show the relationship between the structural parameters (size of QD and inter-dot distance) and the electronic structure. We then show the dependences of TE transport properties on temperature, structural parameters, electronic structure, and chemical potential, and the optimal structural parameters for minimizing the Lorenz number and maximizing ZT in Bi_2Te_3/Sb_2Te_3 QD NCs are identified. Section IV concludes this paper.

II. CARRIER AND PHONON TRANSPORT MODEL

As reviewed in Refs. 6 and 29, tremendous work have been done over the past few years for modeling quantum effects on both electrical transport and phonon transport in QD NCs, with notable contribution from Balandin and co-workers[26,27,28,30,31] and Wang and co-workers.[32,33] Rather than discussing the pros and cons of each individual modeling efforts, the objective of this paper is to identify if there exists structural parameter spaces for optimal thermoelectric properties in QD NCs. We have thus presented here briefly the two-channel

electrical transport model and the modified effective medium approximation model for lattice thermal conductivity that we recently developed for the calculation of TE transport properties of Bi_2Te_3/Sb_2Te_3 QD NCs.[29,34] A distinct feature of the two-channel transport model[29] from the prior works is that both the quantum-confined carriers in minibands and the bulk-like carriers are considered while most of the previous works only consider the quantum-confined electrons in QD NCs. The effect of minibands on ZT would be strongly affected by presence of the bulk-like carriers.

Figure 1 shows the Bi_2Te_3/Sb_2Te_3 QD NCs with spherical Bi_2Te_3 QDs uniformly embedded in an Sb_2Te_3 matrix. The QD size is uniform with a diameter of *a*, and the inter-dot distance is *D*. In QD NCs, some of the electrical carriers could be confined in QDs that form minibands, and the other carriers are bulk-like. Both kinds of carriers transport through the strongly interacting composite that consists of QDs and the matrix. The behavior of the quantum-confined carriers is described by the quantum mechanics model. The overlap of the tails of the electron wave functions that extend from the QDs into the matrix determines the hopping strength between neighboring QDs. A tight-binding model, together with the Kubo formula and the Green's function method, has been developed to study TE transport of quantum-confined carriers. The bulk-like carriers transport through the composite while experiencing carrier-interface scattering at the interfaces between the QDs and the matrix materials. A Boltzmann transport equation (BTE)-based semi-classical transport model is used to describe the multiband transport of bulk-like carriers with both intrinsic carrier scatterings and the carrier-interface scattering.

In our calculation, we assume that the *ab* planes of QDs and matrix are parallel and only

consider the transport in the direction parallel to these *ab* planes of the hexagonal V_2VI_3 lattices. Then the total electronic transport properties can be obtained by simply combining the transport properties of quantum-confined carriers (σ_{QD}, S_{QD}, and $\kappa_{e,\mathrm{QD}}$) with those of bulk-like carriers (σ_{M}, S_{M}, and $\kappa_{e,\mathrm{M}}$) as:

$$\sigma = \sigma_{\mathrm{QD}} + \sigma_{\mathrm{M}}, \tag{4a}$$

$$S = (S_{\mathrm{QD}}\sigma_{\mathrm{QD}} + S_{\mathrm{M}}\sigma_{\mathrm{M}})/(\sigma_{\mathrm{QD}} + \sigma_{\mathrm{M}}), \tag{4b}$$

$$\kappa_e = \kappa_{e,\mathrm{QD}} + \kappa_{e,\mathrm{M}} \quad . \tag{4c}$$

Both electrons and holes contribute to the electrical transport in narrow band gap bulk semiconductors such as Bi_2Te_3 and Sb_2Te_3, so the transport of both the lowest conduction bands and the highest valence bands are considered in calculating bulk-like carrier transport properties. When calculating the transport properties of quantum-confined carriers, we consider only a single-type of carrier for a given type of material [electrons only for *n*-type and holes only for *p*-type] because the carrier concentration decays exponentially with the energy difference between the energy level of holes and energy level of electrons, which is much larger than the band gap of the Bi_2Te_3 bulk material. In Sec. II A and II B, we will present the calculation of transport properties of quantum-confined carriers and bulk-like carriers, respectively. In Sec. II C, the calculation of lattice thermal conductivity will be presented, while Sec. II D presents all the material input parameters used in this study.

A. Transport of quantum-confined carriers

The wave functions of the quantum-confined carriers are calculated by solving the Schrödinger equation with a periodic cosine-shaped confinement potential[29,35] of QD arrays.

The minibands of quantum-confined carriers is described by the Hamiltonian of the tight-binding model:[36]

$$H = \sum_{i,\alpha} E_i c_{i,\alpha}^{+} c_{i,\alpha} - \sum_{i,\alpha,\alpha'} J_i(\mathbf{R}_{\alpha'} - \mathbf{R}_{\alpha}) c_{i,\alpha'}^{+} c_{i,\alpha} = \sum_{i,\mathbf{k}} E_i(\mathbf{k}) c_{i,\mathbf{k}}^{+} c_{i,\mathbf{k}} \,, \tag{5}$$

where $\alpha(\alpha')$ denotes the position of QDs, E_i denotes the *i*th energy level due to the confinement, $c_{i,\alpha}^{+}$ $(c_{i,\alpha})$ is the creation (annihilation) operator at position α, $c_{i,\mathbf{k}}^{+}$ $(c_{i,\mathbf{k}})$ is the creation (annihilation) operator with momentum $\mathbf{k} = (k_x, k_y, k_z)$, and $J_i(\mathbf{R}_{\alpha'} - \mathbf{R}_{\alpha})$ is the overlap integral between QDs that describes the hopping strength. The dispersion relation of the quantum-confined carriers $E_i(\mathbf{k})$ is calculated by the Fourier transformation of the operators:

$$E_i(\mathbf{k}) = E_i - J_i(0) - 2J_i(D\hat{x})\cos(k_x D) - 2J_i(D\hat{y})\cos(k_y D) - 2J_i(D\hat{z})\cos(k_z D) \,, \tag{6}$$

The TE transport properties of the quantum-confined carriers can then be calculated by[37,38]

$$\sigma_{\mathrm{QD}} = \Gamma_{\mathrm{QD}}^{0} \,, \tag{7a}$$

$$S_{\mathrm{QD}} = \Gamma_{\mathrm{QD}}^{1} / T\Gamma_{\mathrm{QD}}^{0} \,, \tag{7b}$$

$$\kappa_{e,\mathrm{QD}} = [\Gamma_{\mathrm{QD}}^{2} - (\Gamma_{\mathrm{QD}}^{1})^2 / \Gamma_{\mathrm{QD}}^{0}] / T \,, \tag{7c}$$

$$\Gamma_{\mathrm{QD}}^{\ell} = N q_j^{2-\ell} \int \frac{dE}{2\pi} (E-\mu)^{\ell} \Xi(E) \left[-\frac{df(E)}{dE} \right], \tag{7d}$$

where q_j is the charge of carrier, $j = (e, h)$ represents electrons and holes, N is the degeneracy of the band, and the superscript $\ell = 0, 1, 2$. $\Gamma_{\mathrm{QD}}^{\ell}$ is the transport coefficient for quantum-confined carriers. The TDF $\Xi(E)$ can be written $\Xi(E) = \sum_i \frac{1}{2\pi^3} \int d\mathbf{k} \left[\partial E_i(\mathbf{k}) / \hbar \partial k_x \right]^2 \delta[E - E_i(\mathbf{k})] \tau_{i,\mathrm{QD}}(E)$,[29] where the total relaxation time ($\tau_{i,\mathrm{QD}}$) is calculated by using the Mathiessen's rule $\frac{1}{\tau_{i,\mathrm{QD}}} = \sum_{\lambda} \frac{1}{\tau_{i,\lambda,\mathrm{QD}}}$. $\tau_{i,\lambda,\mathrm{QD}}$ is the relaxation time of different carrier scattering mechanisms denoted using subscript λ, such as

carrier-acoustic phonon scattering and carrier-optical phonon scattering. Fermi's golden rule is used to calculate the relaxation time of various scattering mechanisms for quantum-confined carriers. The phonon bottleneck effect on the relaxation time is expected for quantum-confined electrons due to the suppression of carrier-phonon scattering according to the momentum and energy conservation rules.[29]

B. Transport of bulk-like carriers

A BTE-based model with the relaxation time approximation is used to study the TE transport properties of bulk-like carriers.[17] We consider the transport of multiband carriers in both the lowest conduction bands and the highest valence bands using the Kane model[39]

$$\frac{\hbar^2 k_{j,\perp}^2}{2m_{j,\perp,\mathrm{M}}^*} + \frac{\hbar^2 k_{j,\parallel}^2}{2m_{j,\parallel,\mathrm{M}}^*} = E_j + \frac{E_j^2}{E_g} \quad . \tag{8}$$

Here $m_{j,\perp,\mathrm{M}}^*$ ($m_{j,\parallel,\mathrm{M}}^*$) is the effective mass of the matrix material perpendicular (parallel) to the *ab* plane of the material, $k_{j,\perp}$ ($k_{j,\parallel}$) is the wave vector, E_j / E_g is the non-parabolicity factor, and E_g is the band gap.

The transport properties of the bulk-like carriers parallel to the *ab* plane are then calculated from the solutions of the linearized BTE with the relaxation time approximation:

$$\sigma = \sum_j \sigma_{j,\mathrm{M}},\ \sigma_{j,\mathrm{M}} = \frac{q_j^2}{3\pi^2 m_{j,\parallel,\mathrm{M}}^*}\left(\frac{2k_B T m_{j,\mathrm{M}}^*}{\hbar^2}\right)^{3/2}\Gamma_{j,\mathrm{M}}^0, \tag{9a}$$

$$S_{\mathrm{M}} = \sum_j S_{j,\mathrm{M}}\sigma_{j,\mathrm{M}} / \sigma,\ S_{j,\mathrm{M}} = \frac{k_B}{q_j}\left(\frac{\Gamma_{j,\mathrm{M}}^1}{\Gamma_{j,\mathrm{M}}^0} - \eta_{j,F}\right), \tag{9b}$$

$$\kappa_{e,\mathrm{M}} = \sum_j \kappa_{e,j,\mathrm{M}},\ \kappa_{e,j,\mathrm{M}} = \frac{k_B}{3\pi^2 m_{j,\parallel,\mathrm{M}}^*}\left(\frac{2k_B T m_{j,\mathrm{M}}^*}{\hbar^2}\right)^{3/2}\left[\Gamma_{j,\mathrm{M}}^2 - \frac{(\Gamma_{j,\mathrm{M}}^1)^2}{\Gamma_{j,\mathrm{M}}^0}\right], \tag{9c}$$

$$\Gamma_{j,\mathrm{M}}^{\ell} = N\int_0^{\infty} \eta_j^{\ell}\gamma^{3/2}(\eta_j)\tau_{j,\mathrm{M}}\left[-\frac{df(\eta_j)}{d\eta_j}\right]d\eta_j, \tag{9d}$$

where $m_{j,\mathrm{M}}^{*} = \left(m_{j,\perp,\mathrm{M}}^{*}m_{j,\|,\mathrm{M}}^{*2}\right)^{1/3}$, k_B is the Boltzmann constant, $\eta_j = E_j / k_B T$, $\eta_{e,F} = (\mu - E_g)/k_B T$, $\eta_{h,F} = -\mu / k_B T$, $\eta_g = E_g / k_B T$, and $\gamma(\eta_j) = \eta_j(1+\eta_j/\eta_g)$, respectively. $\Gamma_{j,\mathrm{M}}^{\ell}$ is the transport coefficient for bulk-like carriers.

The bulk-like carriers experience carrier-interface scattering besides the intrinsic scatterings, all of which have been included in our work through Mathiessen's rule,[17]

$$\frac{1}{\tau_{j,\mathrm{M}}} = \sum_{\lambda'}\frac{1}{\tau_{\lambda',j,\mathrm{M}}} + \frac{1}{\tau_{b,j,\mathrm{M}}}, \tag{10}$$

where λ' denotes the intrinsic carrier scattering mechanisms such as carrier-acoustic phonon scattering, carrier-optical phonon scattering, and carrier-impurity scattering. In Ref. 17, we developed a formula for the relaxation time of carrier-interface scattering as

$$\tau_{b,j,\mathrm{M}} = \frac{\chi_{\mathrm{M}}}{v_{j,\mathrm{M}}}\frac{1}{1-P_j} + \frac{\chi_{\mathrm{QD}}}{v_{j,\mathrm{QD}}}\frac{P_j}{1-P_j}, \tag{11}$$

where $v_{j,\mathrm{M}}(v_{j,\mathrm{QD}})$ is the carrier velocity in the bulk material of matrix (QD) material, χ_{M} (χ_{QD}) is the average distance between two successive scattering events in the matrix (QD), and P_j is the carrier transmission probability at the interface between the matrix and QDs. Physically, Eq. (11) describes the filtering effect of low-energy carrier by interface/boundary scattering. The carriers with energy lower than the barrier height at the interface could be blocked and the carriers with energy higher than the barrier height can easily transport through the interface, with the quantum transmission probability P_j.

C. Lattice Thermal Conductivity

The total thermal conductivity of QD NCs consists of contributions from both electrical

carriers (κ_e) and phonons (κ_p). The electronic thermal conductivity is calculated by Eq. (4c). Due to phonon scattering at the QD-matrix interfaces, the lattice thermal conductivity of QD NCs could be remarkably reduced when the size of QD or the inter-dot distance is smaller than the phonon mean free paths (MFPs) of the constituent materials.[5,6,10,11,12] Furthermore, quantum effects on phonons might further change the lattice thermal conductivity, such as the changes in phonon relaxation time and the phonon dispersion and the resonance phonon scattering, as explore by Balandin and co-workers[30,31] and Wang and co-workers.[32,33] Arguing that the wavelength of dominant heat-carrying phonons in semiconductor at room temperature is only 1-5 nanometers.[40] Phonon BTE-based models which assume incoherent phonon transport for lattice thermal conductivity was developed by Yang and Chen.[10,11,12] To avoid the tedious simulations, the modified effective medium approximation (EMA) model based on the phonon-BTE model[34,41] is recently developed to calculate the lattice thermal conductivity of NCs under the framework of the EMA but with modified lattice thermal conductivity of the matrix and the QDs that takes into account the phonon-interface scattering.[34] We note that currently there are no unanimous understanding on the relative contributions of quantum effects and classical size effects on lattice thermal conductivity on quantum structures such as superlattices and QD NCs and no well-accepted models for calculating the thermal conductivity of these structures accounting both effects.[42] We have thus used the modified EMA model at hand to calculate the lattice thermal conductivity of QD NCs with different QD sizes and inter-dot distances. A slight over-estimate or under-estimate on the lattice thermal conductivity of QD NCs will not change the conclusions of this work. In our calculation, the bulk phonon properties including the lattice thermal

conductivity, the heat capacity, the phonon group velocity, and the phonon MFPs of both constituent materials are required as input parameters for modified EMA.[34,41]

D. Material Input Parameters.

Before we start to study the TE transport of Bi_2Te_3/Sb_2Te_3 QD NCs, it is necessary to obtain the material input parameters of the constituent materials. We first compare the calculated electrical conductivity and Seebeck coefficient in bulk form of both *p*-type Bi_2Te_3 and *p*-type Sb_2Te_3 by using the BTE-based transport model of bulk-like carriers described in Sec II.B (by omitting the interface-scattering of carriers) with the experimental data reported in Ref. 43 as shown in Figs. 2(a) and 2(b) to obtain the input parameters. In our calculation, the highest two valence bands and the lowest two conduction bands of bulk Bi_2Te_3 and bulk Sb_2Te_3 are considered since both Bi_2Te_3 and Sb_2Te_3 are narrow bandgap semiconductors in which both electrons and holes contribute to the bulk-like carrier transport. Due to the negligible band edge offset and the similarity of the effective masses of the two conduction bands,[44,45] we approximate the two conduction bands as degenerate and choose N=12 in the calculation to account for the six pockets of carriers in each band.[17,44] Similar assumption is also made for the two valence bands. The fitting parameters such as the effective masses of electrons and holes, the energy of longitudinal optical phonon $\hbar\omega$, the deformation potential constant φ, the mass density ρ, the static (high-frequency) permittivity ε_s (ε_∞), the sound velocity *c*, and the band gap E_g of Bi_2Te_3 are shown in Table I, and the fitting parameters of Sb_2Te_3 are shown in Table II. Both sets of parameters are in good agreement with the data in the literature.[44,45] In our fitting, we scan the values of the effective mass and the band gap to

match the calculated electrical conductivity and Seebeck coefficient with the experimental data while keeping the other involved parameters to be the same or close to the values in literatures. The experimental doping concentrations $p = 1.1p_0$ in Bi_2Te_3[46] and $p = 8.7p_0$ in Sb_2Te_3[47] are used in the data fitting, where $p_0 = 10^{19}/\mathrm{cm}^3$ throughout the paper.

Although the model established in this paper can be used to calculate the transport properties in both *n*-type and *p*-type QD NCs, we have limited the discussion in this paper to *p*-type materials because the material input parameters we have obtained are based on experimental values of *p*-type materials. As noted earlier, due to the large energy differences between minibands, we consider only a single type of quantum-confined carriers, i.e. holes only for *p*-type QD NCs. Using the hole effective mass of Bi_2Te_3, we obtained (see Table I) and the energy level of holes E_i, we can calculate the overlap integral $J_i(\mathbf{R}_{\alpha'} - \mathbf{R}_{\alpha})$ in Eq. (5) for the given cosine-shaped confinement potential.[29] We choose the height of the confinement potential to be 0.25 eV and choose the valence band offset between QDs and matrix to be 0.08 eV in our calculations. We note that it is really difficult to determine the height of the confinement potential in practice since it depends on the band offset between QDs and matrix materials, the band bending due to depletion effect near the interface, and the surface charge trapping at the interface. The valence band offset between QDs and matrix materials is the summation of the difference of the band gap (0.13-0.14 eV of Bi_2Te_3 and 0.21-0.28eV of Sb_2Te_3 at room temperature[45]) and electron affinity (4.125-4.525 eV of Bi_2Te_3[48] and 4.15eV of Sb_2Te_3[49]). We choose the difference of band gap to be 0.08 eV, and the difference of affinity to be 0.

For calculating the temperature-dependent thermal conductivity of QD NCs, we need

temperature-dependent input parameters. Table III shows the input phonon parameters of the constituent materials such as phonon MFP, phonon group velocity (v_g),lattice thermal conductivity ($\kappa_{p,\text{bulk}}$), and specific heat (c_v) at room temperature (300K) for the calculation of lattice thermal conductivity in QD NCs. The phonon group velocity and specific heat are taken from Ref. 50 and the bulk lattice thermal conductivity is taken from Ref. 51. We approximate the temperature-dependent bulk lattice thermal conductivity by $\kappa_{p,\text{bulk}}(T)/\kappa_{p,\text{bulk}}(300\text{K}) = 300\text{K}/T$, in consistence with the experimental observation that thermal conductivity is inversely proportional to the temperature when $T > 50\text{ K}$.[52] Since the temperatures we consider in this paper (150K-450K) are close to or higher than the Debye temperatures of Bi_2Te_3 (164.9K) and Sb_2Te_3 (160K),[45] we have neglected the temperature-dependences of phonon group velocity and specific heat.[53]

III. RESULTS AND DISCUSSIONS

A. Electronic Minibands and Phonon Bottleneck Effect in Carrier Scattering

In QD NCs, electronic minibands are formed due to the hopping mechanism of quantum-confined carriers. The locations and the bandwidths of the minibands in QD NCs can be tuned by changing the structural parameters, QD size and the inter-dot distance. Figure 3a shows the carrier DOS of minibands for different QD size *a* and inter-dot distance *D* in comparison with the DOS of bulk Sb_2Te_3. The bandwidth of electronic minibands of a QD NC with $(a, D) = (6\text{ nm}, 8.5\text{ nm})$ is 0.065 eV, which is narrower than the 0.1 eV bandwidth of a QD NC with $(a, D) = (6\text{ nm}, 8\text{ nm})$. The bandwidth decreases when the inter-dot distance increases for fixed QD size.

Figure 3(a) also shows the dependence of the chemical potential (μ) on the doping concentration (p), in comparison with the DOS of the miniband in QD NCs with different a and D at room temperature. The doping concentration can be used to shift the chemical potential to be below or above the center of the minibands. For low doping concentration, in which the chemical potential is lower than the center of the minibands, ($E < \mu$), $-df(E)/dE$ in Eq. (7d) increases when the doping concentration increases. A positive S_{QD} and an increasing σ_{QD} are expected with the increasing of doping concentration. For high doping concentration, in which the chemical potential is larger than the center of the miniband ($E > \mu$), a negative S_{QD} and a decreasing σ_{QD} are expected since $-df(E)/dE$ in Eq. (7d) decreases when the doping concentration increases.

Figure 3(b) shows the dependence of bandwidth of quantum-confined carrier minibands on D-a for $a = 6$ nm, 7 nm, and 8 nm. The miniband width monotonically decreases when the inter-dot distance increases because of the reduction of hopping strength. Smaller a leads to larger miniband width because more of the electron wave function tail extends into the matrix.

Figure 3(c) shows the relaxation time of the lowest miniband of quantum-confined carriers (left Y-axis) and the relaxation time of the bulk-like holes (right Y-axis) in QD NCs with different a and D in comparison with the carrier relaxation time in bulk Sb_2Te_3 material. As expected, due to the low-energy carrier filtering effect, the relaxation time of bulk-like carriers is reduced compared to that of the bulk material.[17] However, the relaxation time of quantum-confined carriers could be prolonged for over two orders of magnitude at the upper edge of the minibands due to the phonon bottleneck effect in carrier-phonon scattering.[29] The

competition between the contributions of quantum-confined and bulk-like carriers will dictate the electrical conductivity in QD NCs.

It should be noted that there are two limitations when using the tight-binding model for the quantum-confined carriers: 1) the center of miniband $E_i - J_i(0)$ in Eq. (6), which increases when decreasing *a*, should be smaller than the confinement potential for the electron wave function to be confined in QDs.[29] This means that there is a lower limit of *a* for a given confinement potential to make sure that the solution of the Schrödinger equation exists. In our calculation, this lower limit is about $a = 6$ nm. In other words, when $a < 6$ nm, there exist no quantum-confined carriers in the QDs; 2) The overlap of the electron wave functions between QDs should be close to zero to satisfy the orthogonality of the electron wave functions in the tight-binding model. This second limitation results in a lower limit of *D*-*a* to be 1.5 nm since the overlap of the electron wave function increases when inter-dot distance decreases.

B. TE Transport Properties

In this section we present the dependences of TE transport properties on temperature, doping concentration, and structural parameters (size and inter-dot distance), with the aim of searching for the optimal ZT in Bi_2Te_3/Sb_2Te_3 QD NCs.

Figure 4 shows the temperature dependences of electrical conductivity, Seebeck coefficient, Lorenz number, lattice thermal conductivity, and ZT for different *a* and *D* while fixing the doping concentration at $p = 0.5p_0$, which is close to the optimal doping concentration for QD NCs.[54] Figure 4(a) shows that the electrical conductivity is

significantly higher in QD NCs with $(a, D) = (6\text{ nm}, 8\text{ nm})$, $(6\text{ nm}, 8.5\text{ nm})$, and $(7\text{ nm}, 9\text{ nm})$ than that in bulk Sb_2Te_3, due to the phonon bottleneck effect[29] in the phonon scattering of the quantum-confined carriers. When D becomes smaller, a larger electrical conductivity is expected due to a much stronger hopping strength between QDs. In a QD NC with large inter-dot distance $(a, D) = (6\text{ nm}, 10\text{ nm})$, the electrical conductivity is reduced rather than increased because of the filtering effect of the low-energy bulk-like carriers while the contribution of quantum-confined carriers is not important due to the small hopping strength between QDs. However, the electrical conductivity in a QD NC with small size of QD, $a = 5.5\text{ nm}$, is even smaller than the bulk value since there is no miniband formed when $a < 6\text{ nm}$. Figure 4(b) shows that the Seebeck coefficient in QD NCs with $(a, D) = (6\text{ nm}, 8\text{ nm})$ and $(6\text{ nm}, 8.5\text{ nm})$ is always above $200\ \mu\text{V/K}$. Significant enhancement is shown for a QD NC with $(a, D) = (6\text{ nm}, 8\text{ nm})$ at $T < 225\text{ K}$ and for a QD NC with $(a, D) = (6\text{ nm}, 8.5\text{ nm})$ at $T < 270\text{ K}$; the Seebeck coefficient is even larger than that in Sb_2Te_3 bulk material. Such an enhancement of Seebeck coefficient at low temperature comes from the sharp DOS of the miniband that is located $2.5 \sim 3\, k_B T$ away from the chemical potential. Figures 4(a) and 4(b) together demonstrate simultaneous enhancement of the electrical conductivity and the Seebeck coefficient in a QD NC with $(a, D) = (6\text{ nm}, 8\text{ nm})$ at $T < 225\text{ K}$ and in a QD NC with $(a, D) = (6\text{ nm}, 8.5\text{ nm})$ at $T < 270\text{ K}$, comparing to bulk Sb_2Te_3.

As we discussed in Sec. I, smaller Lorenz number $L = \kappa_e / \sigma T$ is preferred for maximizing ZT. Figure 4(c) shows that the Lorenz numbers in QD NCs with $(a, D) = (6\text{ nm}, 8\text{ nm})$, $(6\text{ nm}, 8.5\text{ nm})$, and $(7\text{ nm}, 9\text{ nm})$ are between

$0.3\times10^{-8} \sim 1.5\times10^{-8}$ WΩ/K^2 , smaller than that in bulk Sb_2Te_3 material, $1.8\times10^{-8} \sim 2.05\times10^{-8}$ WΩ/K^2, due to the dominance of the quantum-confined carrier transport channel in QD NCs. It is also shown that the Lorenz number in a QD NC with $(a, D) = (6\text{ nm}, 8.5\text{ nm})$ is smaller than both the $(6\text{ nm}, 8\text{ nm})$ and $(6\text{ nm}, 10\text{ nm})$ cases when $T < 350$ K. Clearly there exists a minimum of Lorenz number when we change the inter-dot distance for a fixed QD size, due to the competition between the bulk-like carrier transport channel and the quantum-confined carrier transport channel. For bulk-like carriers, $\kappa_{e,\mathrm{M}} / \sigma_{\mathrm{M}} T$ could be larger than the Lorenz number in bulk Sb_2Te_3 material due to the change of the energy dependence of scattering mechanisms induced by the low-energy carrier filtering effect.[17] For quantum-confined carriers, the decrease of inter-dot distance for a fixed QD size results in an increase of the bandwidth, which in turn increases $\kappa_{e,\mathrm{QD}} / \sigma_{\mathrm{QD}} T$. Therefore, the minimum of the Lorenz number occurs when the contribution of the quantum-confined carrier transport channel overcomes the contribution of the bulk-like carrier transport channel. The presence of bulk-like carriers would significantly change the effect of minibands on the TE transport.

Figure 4(d) shows the significantly reduced lattice thermal conductivity in QD NCs due to phonon scattering at the interface between QDs and matrix. At room temperature, the lattice thermal conductivity can be reduced from 1.7W/mK in bulk material to 0.4-0.7W/mK in QD NCs. As expected, smaller *a* or *D* results in lower lattice thermal conductivity. Figure 4(e) shows an enhanced ZT when the reduction of denominator in Eq. (2) ($L + \kappa_p / \sigma T$) overwhelms the slight decrease of the Seebeck coefficient in numerator shown in Fig. 4(b). The maxima of enhanced ZT are found to be ~7.6 at $T > 450$ K in a QD NC with

$(a, D) = (6\ \text{nm}, 8\ \text{nm})$, to be ~3.5 at $T = 300\ \text{K}$ for $(a, D) = (6\ \text{nm}, 8.5\ \text{nm})$, and to be ~3.9 at $T = 380\ \text{K}$ for $(a, D) = (7\ \text{nm}, 9\ \text{nm})$. The ZT values in QD NCs with small size of QD $(a, D) = (5.5\ \text{nm}, 7.5\ \text{nm})$ and large inter-dot distance $(a, D) = (6\ \text{nm}, 10\ \text{nm})$ are close to the ZT in bulk Sb_2Te_3 because the transport by quantum-confined carriers is small.

Figure 5 shows the dependences of TE transport properties on the doping concentration (p) in QD NCs for different a and D at $T = 300\ \text{K}$. Figure 5(a) shows that there is an optimum doping for electrical conductivity in QD NCs with $(a, D) = (6\ \text{nm}, 8\ \text{nm})$, $(6\ \text{nm}, 8.5\ \text{nm})$, and $(7\ \text{nm}, 9\ \text{nm})$. In contrast, the electrical conductivity monotonically increases with the doping concentration in bulk Sb_2Te_3 and in QD NCs with small size of QD $(a, D) = (5.5\ \text{nm}, 7.5\ \text{nm})$ or with large inter-dot distance $(a, D) = (6\ \text{nm}, 10\ \text{nm})$. These different dependences of electrical conductivity on the doping concentration come from the shift of chemical potential when the doping concentrations change, as shown in Fig. 3(a). The total electrical conductivity $\sigma = \sigma_{\text{QD}} + \sigma_{\text{M}}$: 1) for QDs with $(a, D) = (6\ \text{nm}, 8\ \text{nm})$ increases first and then decreases since the quantum-confined carriers dominate the transport; 2) for QDs with $(a, D) = (5.5\ \text{nm}, 7.5\ \text{nm})$ and $(6\ \text{nm}, 10\ \text{nm})$ always increases since the bulk-like carriers dominate the transport; 3) for QDs with $(a, D) = (6\ \text{nm}, 8.5\ \text{nm})$ and $(7\ \text{nm}, 9\ \text{nm})$ increases first and then decreases at the low doping concentration since the quantum-confined carriers dominate the transport at low doping concentration, but increases again since the bulk-like carriers dominate the transport for high doping concentration. The shift of the chemical potential when the doping concentration changes as shown in Fig. 3(a) could also result in a sign change of Seebeck coefficient. Figure 5(b) shows that the Seebeck coefficient decreases with the increase of doping concentration until reaching a negative

minimum value and then increasing for $(a, D) = (6\text{ nm}, 8.5\text{ nm})$, $(6\text{ nm}, 8.5\text{ nm})$, and $(7\text{ nm}, 9\text{ nm})$ cases, and is always positive for $(a, D) = (5.5\text{ nm}, 7.5\text{ nm})$ and $(6\text{ nm}, 10\text{ nm})$. The total Seebeck coefficient $S = (S_{\text{QD}}\sigma_{\text{QD}} + S_{\text{M}}\sigma_{\text{M}})/\sigma$ is positive for low doping concentrations and could be negative at high doping concentrations because the quantum-confined carriers with negative Seebeck coefficient dominate the transport.

Figure 5(c) shows that the Lorenz numbers in QD NCs with $(a, D) = (6\text{ nm}, 8\text{ nm})$, $(6\text{ nm}, 8.5\text{ nm})$, and $(7\text{ nm}, 9\text{ nm})$ are between $0.3\times10^{-8} \sim 0.7\times10^{-8}\ \text{W}\Omega/\text{K}^2$, much smaller than in Sb_2Te_3 bulk material, $1.8\times10^{-8} \sim 2.4\times10^{-8}\ \text{W}\Omega/\text{K}^2$, for low doping concentration ($p < 4p_0$) when the quantum-confined carriers dominate the transport. For larger doping concentration, the Lorenz numbers become closer to the bulk values when the bulk-like carriers become important. When the QD size is too small or the inter-dot distance is too large, the Lorenz numbers in QD NCs could be even larger than in Sb_2Te_3 bulk material, as shown in the cases of $(a, D) = (5.5\text{ nm}, 7.5\text{ nm})$ and $(a, D) = (6\text{ nm}, 10\text{ nm})$.

Figure 5(d) shows the doping concentration of ZT in QD NCs with $(a, D) = (6\text{ nm}, 8\text{ nm})$, $(6\text{ nm}, 8.5\text{ nm})$, and $(7\text{ nm}, 9\text{ nm})$. The maximum ZT reaches ~6.8 when the doping concentration is $0.2\ p_0$ and reaches ~1.2 when the doping concentration is $10\ p_0$ in a QD NC with $(a, D) = (6\text{ nm}, 8\text{ nm})$. The former maximum ZT comes from the simultaneous reduction of Lorenz number and the lattice thermal conductivity. The latter ZT is much smaller than the former one because its Seebeck coefficient is much smaller due to cancellation between the negative S_{QD} and the positive S_{M}, and because the Lorentz number at high doping concentration is not significantly lower than its bulk value. In addition, the optimal doping concentration changes from $0.2\ p_0$ to p_0 when inter-dot distance

increases from 8 nm to 10 nm and $a = 6$ nm.

It was shown that the Lorenz number in a QD NC with $(a, D) = (6\text{ nm}, 8\text{ nm})$ is smaller than in both the $(a, D) = (6\text{ nm}, 8.5\text{ nm})$ and $(6\text{ nm}, 10\text{ nm})$ cases when $T < 350$ K for $p = 0.5\ p_0$ in Fig. 4(c) and for $p < 4\ p_0$ at $T = 300$ K in Fig. 5(c). To search for the optimal structural parameters to minimize the Lorenz number, Figure 6(a) shows the bandwidth dependences of the Lorenz number and $L + \kappa_p / \sigma T$ for different size of QD at $a = 6$ nm and 7 nm in comparison with the Sb_2Te_3 bulk material when $T = 300$ K and $p = 0.5 p_0$. When the bandwidth is close to zero, which means that the bulk-like carriers are dominant, slight increases of Lorenz number is found. The minimum of the Lorenz number is found at a bandwidth of $2.4 k_B T$ for both the $a = 6$ nm and $a = 7$ nm cases. However, the minimum of $L + \kappa_p / \sigma T$ is shifted to a bandwidth of $3.2 k_B T$ for $a = 6$ nm and to $4.4 k_B T$ for $a = 7$ nm.

The minimum of Lorenz number which comes from the competition between the quantum-confined carriers and bulk-like carriers strongly affect ZT. Figures 6(b) and 6(c) show the dependence of ZT on the bandwidth and inter-dot distance for different QD size and doping concentrations at $T = 300$ K. The maxima of ZT are found: 1) when the bandwidth equals to $3.9 k_B T$ (*D*-*a* equals to 2 nm) for $a = 6$ nm and $p = 0.5 p_0$; 2) when the bandwidth equals to $3.2 k_B T$ (*D*-*a* equals to 2.3 nm) for $a = 6$ nm and $p = p_0$; 3) when the bandwidth equals to $3.1 k_B T$ (*D*-*a* equals to 1.7 nm) for $a = 7$ nm and $p = 0.5 p_0$. These maxima of ZT with bandwidth are consistent with the minimum of $L + \kappa_p / \sigma T$ shown in Fig. 6(a). Figure 6(d) shows ZT as a function of the chemical potential for different inter-dot distances at $T = 300$ K when $a = 6$ nm. We find that the optimal ZT shifts to

higher chemical potential, and the value of ZT decreases when the inter-dot distance increases.

In Fig. 6 we clearly show that there exist optimal structural parameters that result in optimal bandwidth to maximize ZT in Bi_2Te_3/Sb_2Te_3 QD NCs. When QD size $a = 6$ nm and *D-a* is around 2 nm, the ZT reaches its maximum due to the minimization of the Lorentz number and the reduction of the lattice thermal conductivity.

VI. CONCLUSIONS

From the existence of an optimal bandwidth in a narrow conduction band for maximizing the thermoelectric figure of merit, we performed detailed calculations in this paper to search for the optimal ZT in Bi_2Te_3/Sb_2Te_3 quantum dot nanocomposites with Bi_2Te_3 QDs uniformly embedded in a Sb_2Te_3 matrix. A two-channel electrical transport model that includes both the narrow miniband transport by the quantum-confined carriers and the background transport by the bulk-like carriers was used to calculate the electrical transport properties in QD NCs, and the modified effective medium approximation model was used for the phonon transport. Simultaneous decrease of the lattice thermal conductivity and the Lorenz number leads to an enhanced ZT in QD NCs when the Seebeck coefficient is slightly decreased. The optimal structural parameters that induce an optimal electronic structure to maximize ZT with the consideration of the detailed scattering physics, including phonon bottleneck effect, are found in this composite material system. The optimal QD size was found to be 6 nm while the optimal inter-dot distance depends on the QD size and the doping concentration. For a fixed QD size, the maximum ZT is obtained at the minimum of

Lorenz number, which occurs when the quantum-confined carrier transport overwhelms the background transport from the bulk-like carriers.

ACKNOWLEDGMENTS

We would like to thank Mr. Xiaobo Li and Dr. Jose Ordonez-Miranda for their assistance with the lattice thermal conductivity calculations. This work is supported by DARPA (Contract N66001-10-C-4002, managed by Dr. Thomas Kenny and Dr. Avi Bar-Cohen) and NSF (Grant No. CBET 0846561).

Table I. Parameters used to calculate the carrier transport coefficients for Bi_2Te_3.

PARAMETERS	VALUE	PARAMETERS	VALUE
$m^*_{h,\mathrm{QD}}$ (m_0)	0.08[a]	$\hbar\omega$ (meV)	13[b]
c (km/s)	2.95[a]	φ (eV)	15[c]
ρ (g/cm^3)	7.86[a]	$\varepsilon_s(\varepsilon_0)$ [d]	168[e]
$\varepsilon_\infty(\varepsilon_0)$ [d]	50[f]	E_g (meV)	130[g]

[a] in Ref. 45.

[b] 6.2~14.9 in Ref. 45.

[c] 9.5 in Ref. 45, 35~40 in Ref. 44.

[d] ε_0 is the permittivity of free space.

[e] 75~290 in Ref. 45.

[f] 50~85 in Ref. 45.

[g] Ref. 45, room temperature.

Table II. Parameters used to calculate the carrier transport coefficients for Sb_2Te_3.

PARAMETERS	VALUE	PARAMETERS	VALUE
$m^*_{h,\mathrm{M}}$ (m_0)	0.057[a]	$\hbar\omega$ (meV)	13[b]
$m^*_{e,\mathrm{M}}$ (m_0)	0.057	φ (eV)	15
c (km/s)	2.9[a]	$\varepsilon_s(\varepsilon_0)$ [c]	168[d]
ρ (g/cm^3)	6.505[a]	$\varepsilon_\infty(\varepsilon_0)$ [c]	30[e]
E_g (meV)	210[f]		

[a] in Ref. 45.

[b] 9.6~20.9 in Ref. 45.

[c] ε_0 is the permittivity of free space.

[d] 36.5~168 in Ref. 45.

[e] 29.5~53 in Ref. 45.

[f] Ref. 45, room temperature.

Table III. Parameters at room temperature used to calculate the lattice thermal conductivity of QD NCs.

MATERIAL	$\kappa_{p,\mathrm{bulk}}$ (W/mK)	$c_v 10^6$(J/ m^{3}K)	v_g (m/s)	MFP (nm)
Bi_2Te_3	1.55	0.5	212	43.7
Sb_2Te_3	1.7	0.53	200	48

FIGURE CAPTIONS

FIG 1. (Color online) Schematic diagram of the Bi_2Te_3/ Sb_2Te_3 QD NCs with spherical Bi_2Te_3 QDs with size *a* uniformly embedded in Sb_2Te_3 matrix material with inter-dot distance *D*.

FIG 2. (Color online) (a) Electrical conductivity and (b) Seebeck coefficient, of *p*-type Bi_2Te_3 and *p*-type Sb_2Te_3 bulk materials plotted as a function of temperature in comparison with the experimental data reported in Ref. 43. The doping concentration of Bi_2Te_3 is $p = 1.1p_0$ and that of Sb_2Te_3 is $p = 8.7p_0$, where $p_0 = 10^{19}/\mathrm{cm}^3$.

FIG 3. (Color online) (a) The DOS (left Y-axis) of electronic minibands in QD NCs with different size of QD and different inter-dot distance, and the DOS of bulk Sb_2Te_3 material. The relationship of the doping concentration (*p*, right Y-axis) and the chemical potential (μ) is also plotted for comparison. (b) Bandwidth of quantum-confined carrier miniband (W_b) plotted as a function of inter-dot distance for different size of QD with $a = 6$ nm, 7 nm, and 8 nm. (c) Relaxation time of the lowest miniband of quantum-confined carriers ($\tau_{1,QD}$, left Y-axis) and bulk-like holes ($\tau_{h,M}$, right Y-axis) in QD NCs with $(a, D) = (6\ \mathrm{nm}, 8\ \mathrm{nm})$, $(6\ \mathrm{nm}, 8.5\ \mathrm{nm})$, and $(7\ \mathrm{nm}, 9\ \mathrm{nm})$, in comparison with the carrier relaxation time in bulk Sb_2Te_3 bulk material.

FIG 4. (Color online) Temperature dependence of (a) electrical conductivity, (b) Seebeck coefficient, (c) Lorenz number, (d) lattice thermal conductivity, and (e) ZT, for Bi_2Te_3/Sb_2Te_3 QD NCs with different QD size *a* and inter-dot distance *D* when $p = 0.5p_0$.

Calculated transport properties for *p*-type Sb_2Te_3 bulk material are also presented for comparison.

FIG 5. (Color online) The dependence of (a) electrical conductivity, (b) Seebeck coefficient, (c) Lorenz number, and (d) ZT, on the doping concentration for Sb_2Te_3/Bi_2Te_3 QD NCs with $a = 6$ nm and different inter-dot distance D at $T = 300$ K. Calculated transport properties for *p*-type Sb_2Te_3 bulk material are also presented for comparison.

FIG 6. (Color online) (a) Lorenz number (L, left Y-axis) and $L + \kappa_p / \sigma T$ (right Y-axis) plotted as a function of the electronic miniband width for QD NCs with different size a of QDs in comparison with the bulk Sb_2Te_3 value when $T = 300$ K and $p = 0.5 p_0$. (b) Bandwidth dependence and (c) D-a dependence of ZT for QD NCs with different size of QD and different doping concentration at $T = 300$ K. (d) The dependence of ZT on the chemical potential for QD NCs with $a = 6$ nm and different inter-dot distances at $T = 300$ K.

Figure 1

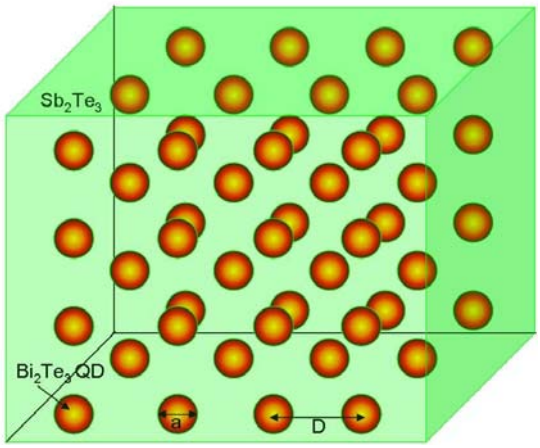

Figure 2

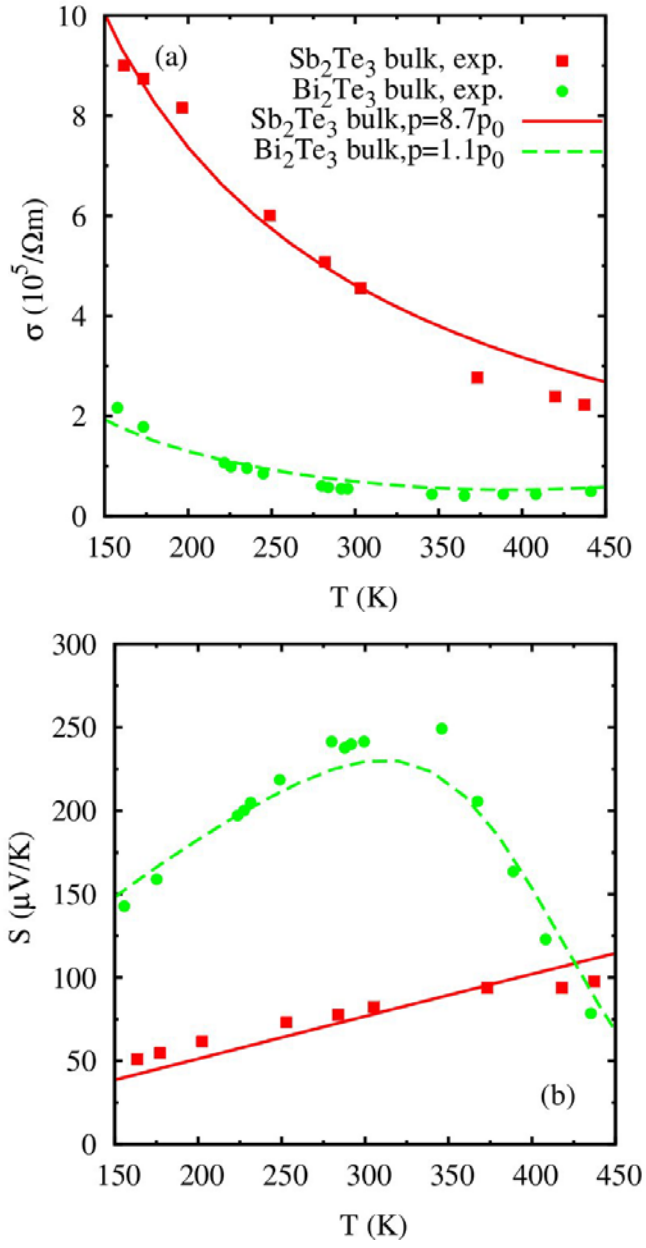
(a)
Sb2Te3 bulk, exp.
Bi2Te3 bulk, exp.
Sb2Te3 bulk,p=8.7p0
Bi2Te3 bulk,p=1.1p0
σ (10^5/Ωm)
T (K)
(b)
S (μV/K)
T (K)

Figure 3

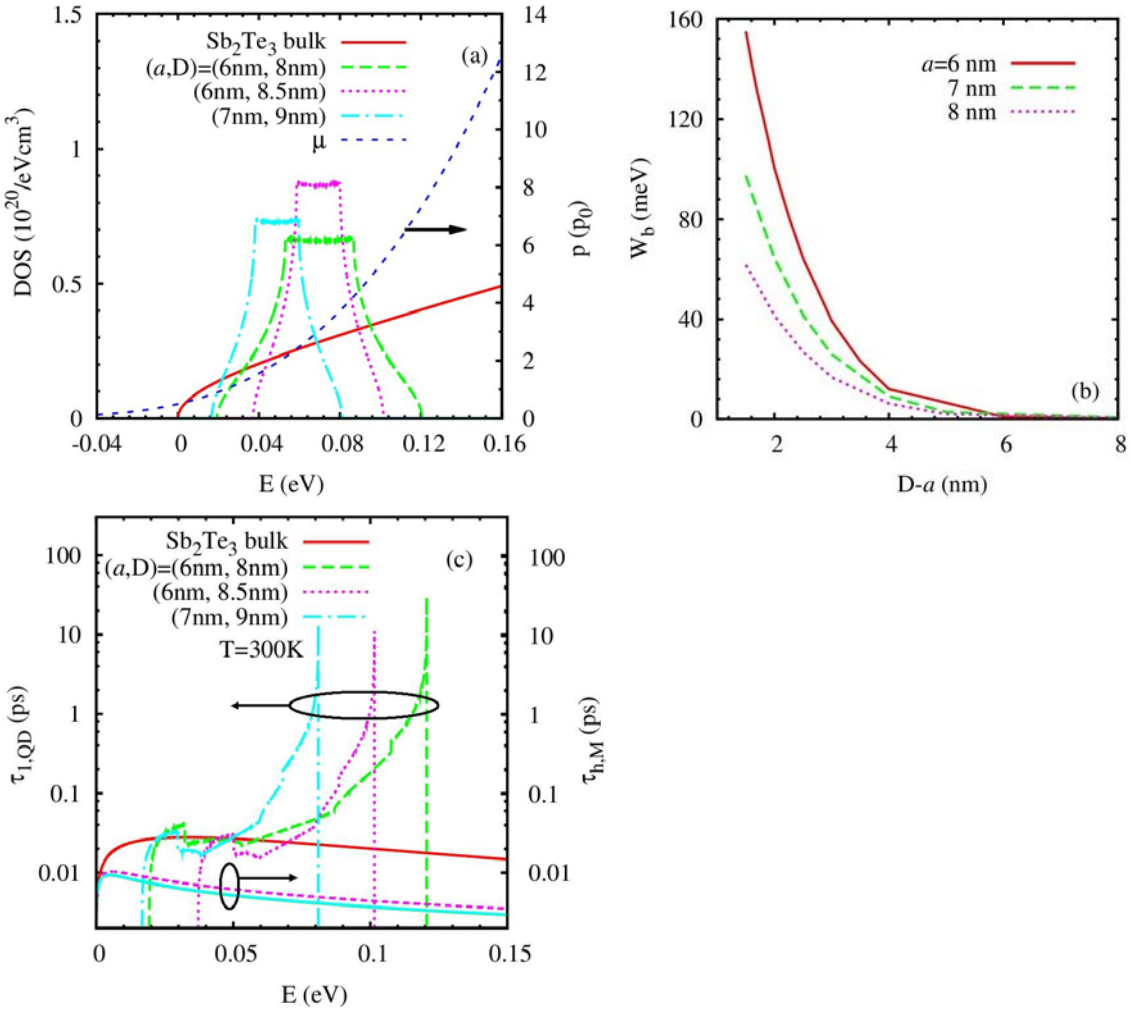
Sb2Te3 bulk
(a,D)=(6nm, 8nm)
(6nm, 8.5nm)
(7nm, 9nm)
μ
(a)
DOS (10^20/eVcm^3)
p (p0)
E (eV)
a=6 nm
7 nm
8 nm
(b)
Wb (meV)
D-a (nm)
Sb2Te3 bulk
(a,D)=(6nm, 8nm)
(6nm, 8.5nm)
(7nm, 9nm)
T=300K
(c)
τ1,QD (ps)
τh,M (ps)
E (eV)

Figure 4

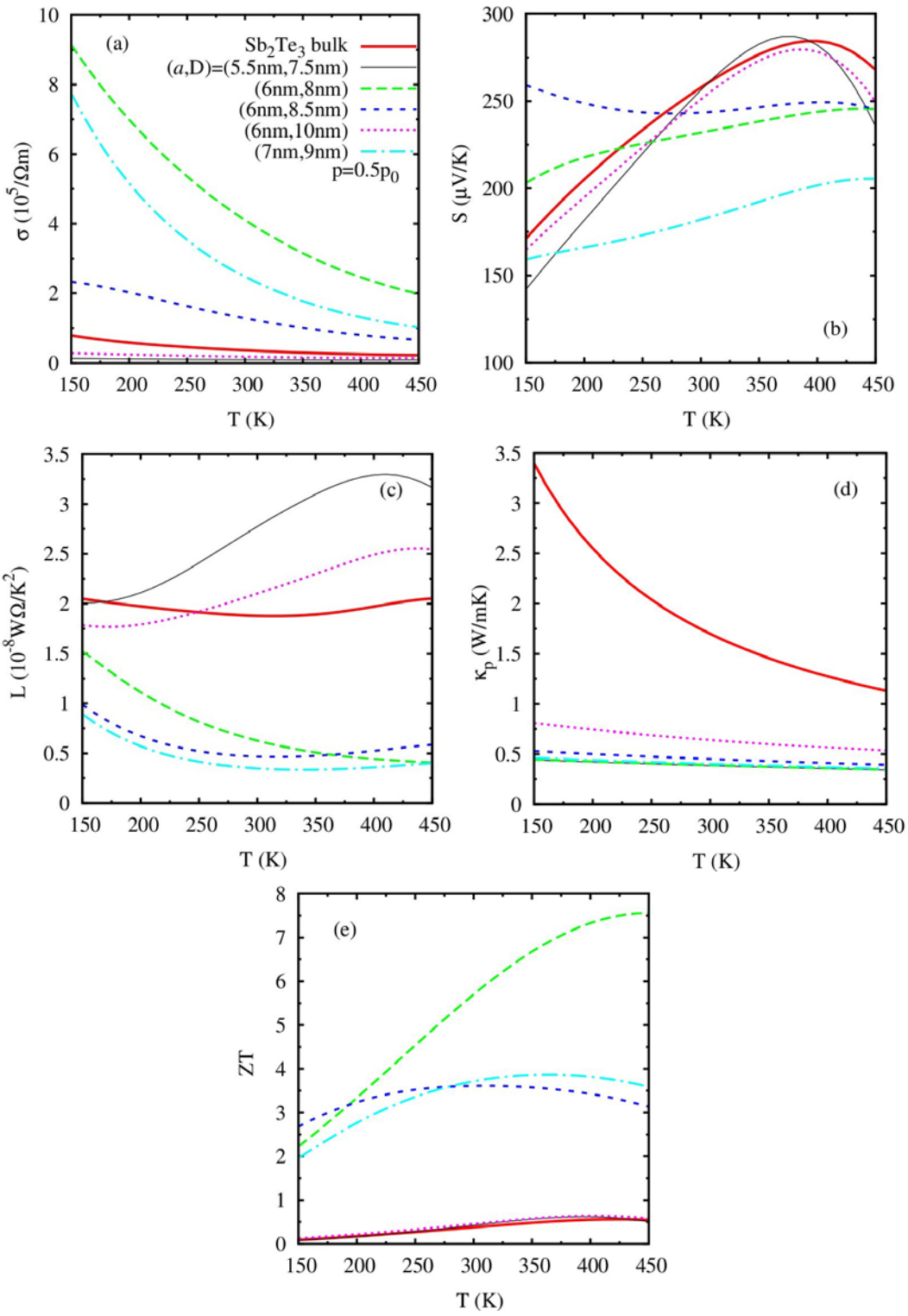
(a)
Sb2Te3 bulk
(a,D)=(5.5nm,7.5nm)
(6nm,8nm)
(6nm,8.5nm)
(6nm,10nm)
(7nm,9nm)
p=0.5p0
σ (10^5/Ωm)
T (K)
(b)
S (μV/K)
T (K)
(c)
L (10^-8WΩ/K^2)
T (K)
(d)
κp (W/mK)
T (K)
(e)
ZT
T (K)

Figure 5

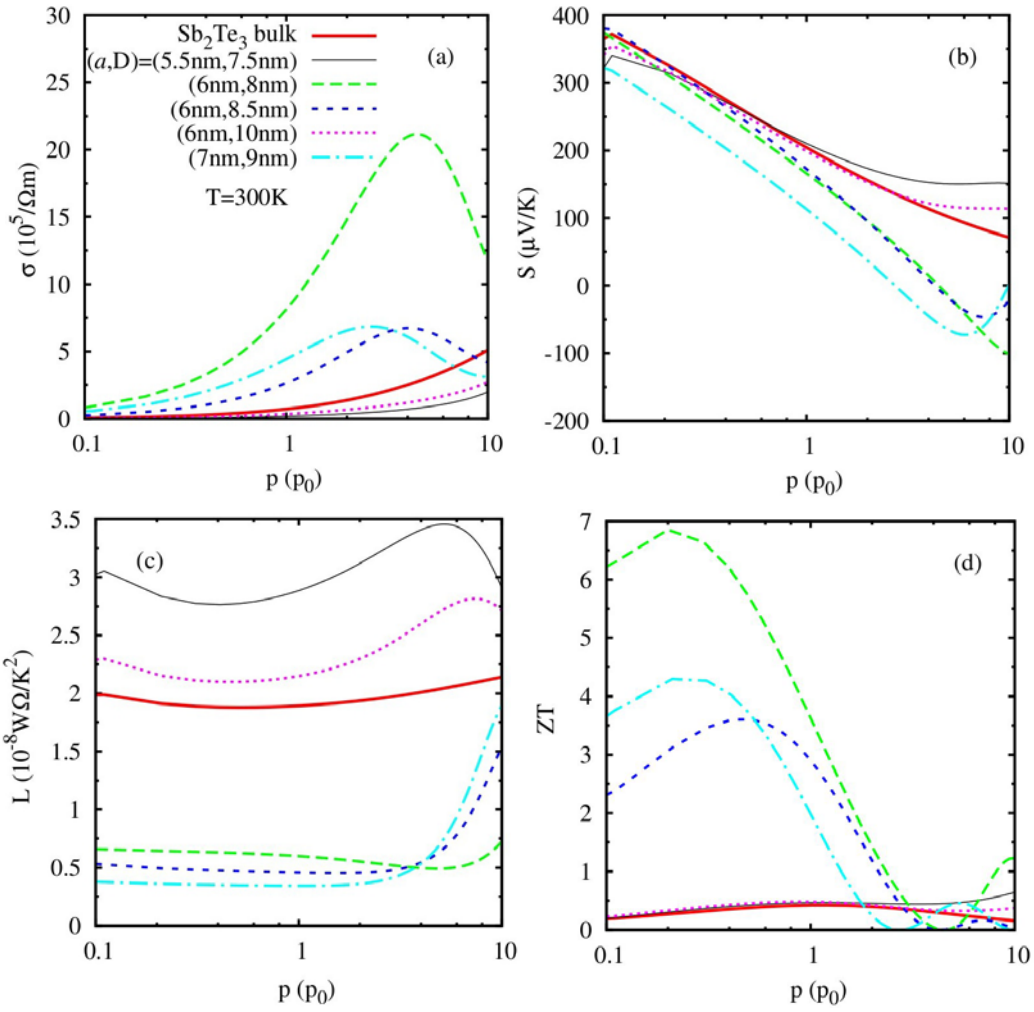
Sb2Te3 bulk
(a,D)=(5.5nm,7.5nm)
(6nm,8nm)
(6nm,8.5nm)
(6nm,10nm)
(7nm,9nm)
T=300K
(a)
σ (10^5/Ωm)
p (p0)
(b)
S (μV/K)
(c)
L (10^-8WΩ/K^2)
(d)
ZT

Figure 6

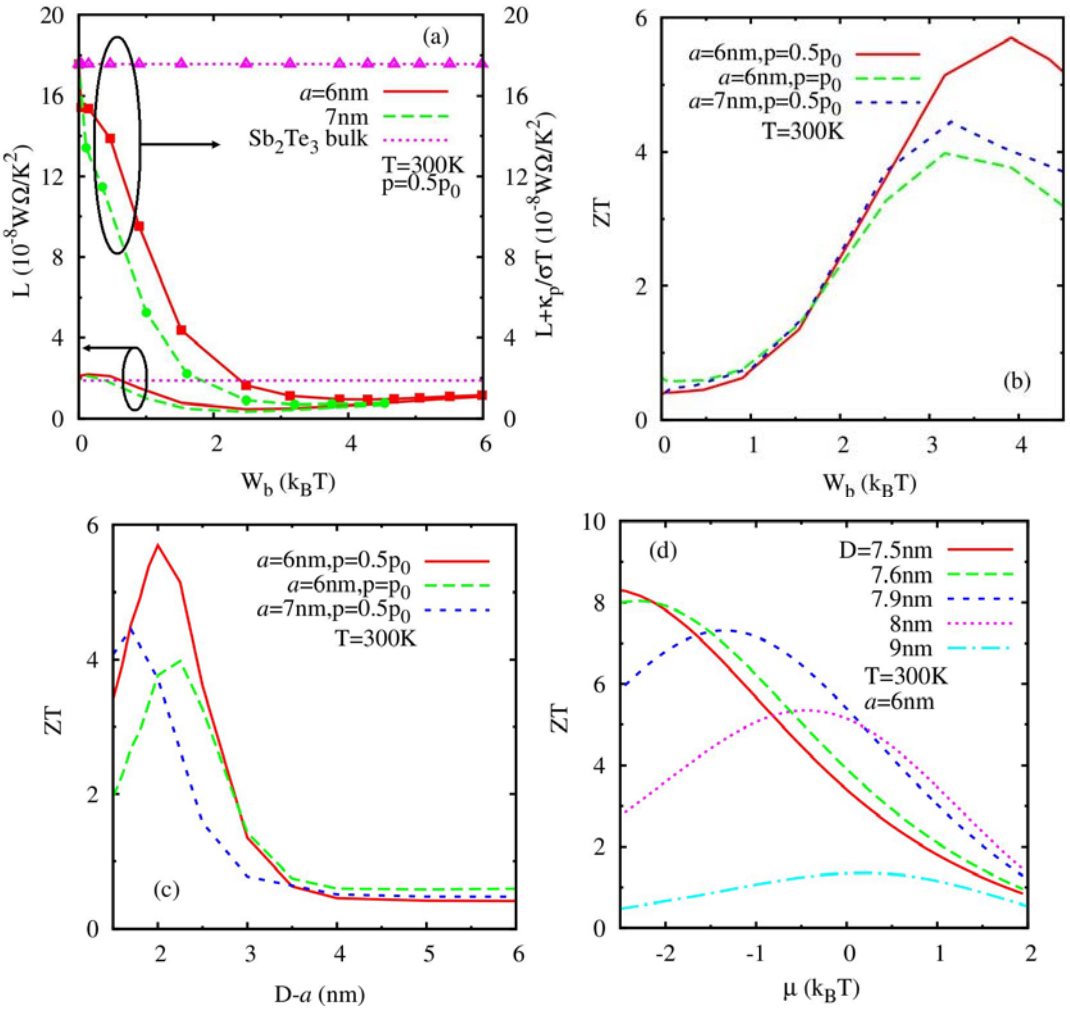
(a)
a=6nm
7nm
Sb2Te3 bulk
T=300K
p=0.5p0
L (10^-8 WΩ/K^2)
L+κp/σT (10^-8 WΩ/K^2)
Wb (kBT)
(b)
a=6nm,p=0.5p0
a=6nm,p=p0
a=7nm,p=0.5p0
T=300K
ZT
Wb (kBT)
(c)
a=6nm,p=0.5p0
a=6nm,p=p0
a=7nm,p=0.5p0
T=300K
ZT
D-a (nm)
(d)
D=7.5nm
7.6nm
7.9nm
8nm
9nm
T=300K
a=6nm
ZT
μ (kBT)

References

1 M. S. Dresselhaus, G. Chen, M. Y. Tang, R. G. Yang, H. Lee, D. Z. Wang, Z. F. Ren, J. P. Fleurial, and P. Gogna, Adv. Mater. **19**, 1043 (2007).

2 L. E. Bell, Science **321**, 1457 (2008).

3 H. J. Goldsmid, *Electronic Refrigeration*, (Pion, London, 1986).

4 D. M. Rowe, in *Thermoelectric Handbook: Macro to Nano*, edited by D. M. Rowe (Taylor & Francis Group, Boca Raton, 2006), p. 1-9.

5 G. Chen, Phys. Rev. B. **57**, 14958 (1998).

6 R.G. Yang and G. Chen, Phys. Rev. B **69**, 195316 (2004).

7 W. Kim, J. Zide, A. Gossard, D. Klenov, S. Stemmer, A. Shakouri, A. Majumdar, Phys. Rev. Lett. **96**, 045901 (2006).

8 B. Poudel, Q. Hao, Y. Ma, Y. C. Lan, A. Minnich, B. Yu, X. Yan, D. Z. Wang, A. Muto, D. Vashaee, X. Y. Chen, J. M. Liu, M. S. Dresselhaus, G. Chen, and Z. F. Ren, Science **320**, 634 (2008).

9 R. Venkatasubramanian, E. Siivola, T. Colpitts, and B. O'Quinn, Nature **413**, 597 (2001).

10 R. G. Yang, G. Chen, and M. S. Dresselhaus, Phys. Rev. B **72**, 125418 (2005).

11 M. S. Jeng, R. G. Yang, D. W. Song, and G. Chen, ASME J. Heat Trans. **130**, 042410 (2008).

12 W. X. Tian and R. G. Yang, J. Appl. Phys. **101**, 054320 (2007).

13 B. C. Sales, D. Mandrus, and R. K. Williams, Science **272**, 1325 (1996).

14 R. P. Hermann, R. Jin, W. Schweika, F. Grandjean, D. Mandrus, B. C. Sales, and G. J. Long, Phys. Rev. Lett. **90**, 135505 (2003).

15 G. D. Mahan and J. Sofo, Proc. Natl. Acad. Sci. USA **93**, 7436 (1996).

16 J. Lee, J. Wu, and J. C. Grossman, Phys. Rev. Lett. **104**, 016602 (2010).

17 J. Zhou, X. B. Li, G. Chen, and R. G. Yang, Phys. Rev. B **82**, 115308 (2010).

18 Z. Fan, H. Wang, and J. Zheng, J. Appl. Phys. **109**, 073713 (2011).

19 C. Jeong, R. Kim, and M. Lundstrom, arXiv:1103.1274v1, (2011).

20 P. Pichanusakorn and P. R. Bandaru, Appl. Phys. Lett. **94**, 223108 (2009).

21 R. Franz and G. Wiedemann, Annalen der Physik **165**, 497 (1853).

22 Z. Bian, M. Zebarjadi, R. Singh, Y. Ezzahri, A. Shakouri, G. Zheng, J. Bahk, J. E. Bowers, J. M. O. Zide, and A. C. Gossard, Phys. Rev. B **76**, 205311 (2007).

23 F. Völklein, H. Reith, T. W. Cornelius, M. Rauber, and R. Neumann, Nanotechnology **20**, 325706 (2009).

24 J. M. Steele, The Cauchy-Schwarz Master Class: An Introduction to The Art of Mathematical Inequalities, (Cambridge University Press, Cambridge, 2004).

25 J. Zhou, R. G. Yang, G. Chen, and M. S. Dresselhaus, Phys. Rev. Lett. **107**, 226601 (2011).

26 A. A. Balandin and O. L. Lazarenkova, Appl. Phys. Lett. **82**, 415 (2003).

27 O. L. Lazarenkova and A. A. Balandin, Phys. Rev. B **66,** 245319 (2002).

28 O. L. Lazarenkova and A. A. Balandin, J. Appl. Phys. **89**, 5509 (2001).

29 J. Zhou and R. G. Yang, J. Appl. Phys. **110**, 084317 (2011).

30 M. Shamsa, W. L. Liu, A. A. Balandin, and J. L. Liu, Appl. Phys. Lett. 87, 202105 (2005).

31 Y. Bao, W. L. Liu, M. Shamsa, K. Alim, A. A. Balandin, and J. L. Liu, J. Electrochemical Society 152, G432 (2005).

32 A. Khitun, A. A. Balandin, J. L. Liu, and K. L. Wang, J. Appl. Phys. **88**, 696 (2000).

33 A. Khitun, A. A. Balandin, J. L. Liu, and K. L. Wang, Superlattices and Microstructures **30**, 1 (2001).

34 J. Ordonez-Miranda, R. G. Yang, and J. J. Alvarado-Gil, Appl. Phys. Lett. **98**, 233111 (2011).

35 H. Tamura, K. Shiraishi, T. Kimura, and H. Takayanigi, Phys. Rev. B **65**, 085324 (2002).

36 N. W. Ashcroft and N. D. Mermin, *Solid State Physics*, (Thomson Lerning, Inc. 1976).

37 J. Zhou and R. G. Yang, Phys. Rev. B **82**, 075324 (2010).

38 C. Grenzebach, F. B. Anders, G. Czycholl, and T. Pruschke, Phys. Rev. B **74**, 195119 (2006).

39 B. R. Nag, *Electron Transport in Compound Semiconductors* (Springer-Verlag, Berlin, 1980).

40 G. Chen, D. Borca-Tascuic and R.G. Yang, *Nanoscale Heat Transfer*, in Encyclopedia of Nanoscience and Nanotechnology, edited by H.S. Nalwa, (American Scientific Publishers, New York, 2004).

41 A. Minnich and G. Chen, Appl. Phys. Lett. **91**, 073105 (2007).

42 B. Yang and G. Chen, Phys. Rev. B **67**, 195311 (2003).

43 H. W. Jeon, H. P. Ha, D. B. Hyun, and J. D. Shim, J. Phys. Chem. Solids **52**, 579 (1991).

44 B. L. Huang and M. Kaviany, Phys. Rev. B **77**, 125209 (2008).

45 *Non-Tetrahedrally Bonded Elements and Binary Compounds I* , Landolt-Börnstein Vol.III/41C, edited by O. Madelung, U. Rössler, and M. Schulz (Springer-Verlag, Berlin, 1998).

46 M. Stordeur, *Valence Band Structure and the Thermoelectric Figure-of-Merit of $(Bi_{1-x}Sb_x)_2Te_3$ Crystals*, in CRC Handbook of Thermoelectrics, edited by D. W. Rowe (CRC Press, Boca Raton, 1995).

47 M. S. Park, J. H. Song, J. E. Medvedeva, M. Kim, I. G. Kim, and A. Freeman, Phys. Rev. B **81**, 155211 (2010).

48 J. Nagao, E. Hatta, and K. Mukasa, in Proceedings of the 15th International Conference on Thermoelectric, 1996 (IEEE Service Center, Piscataway, NJ, 1996), p. 404.

49 M. A. Matin, M. M. Aliyu, A. H. Quadey, and N. Amin, Sol. Energy Mater. Sol. Cells **94**, 1496 (2010).

50 A. Pattamatta and C. K. Madnia, Int. J. Heat Mass Trans. **52**, 860 (2009).

51 H. J. Goldsmid, J. Appl. Phys. **32**, 2198 (1961).

52 P. A. Walker, Proc. Phys. Soc. (London) **76**, 113 (1961).

53 For example, the heat capacity at 150 K is only 6% smaller than that at 300 K which does not significantly affect the calculated lattice thermal conductivity.

54 As shown in Figure 5(d) of Section III. B, the optimal doping concentration in QD NCs is significantly lower than that in bulk Sb_2Te_3 material and changes with the structural parameters of the QD NCs.